RSC Advances

PAPER

Cite this: *RSC Adv.*, 2016, **6**, 4705

Size evolution and ligand effects on the structures and stability of $(AuL)_n$ (L = Cl, SH, SCH_3, PH_2, $P(CH_3)_2$, n = 1–13) clusters†

Yao Liu, Zhimei Tian and Longjiu Cheng*

The synthesis and characterization of ligand protected gold nanoclusters (Au_mL_n) have attracted great interest. After the crystallization of $Au_{102}(SR)_{44}$ and $Au_{25}(SR)_{18}^-$ clusters, the syntheses and theoretical predictions of Au_mL_n clusters have been greatly accelerated. To date, there are few systematic studies on the size evolution and ligand effects of Au–L binary systems. Herein, using a stoichiometric $(AuL)_n$ (n = 1–13) system as a test case, we theoretically investigate the ligand effects (L = Cl, SH, SCH_3, PH_2, and $P(CH_3)_2$) on these structures and size evolution. The method of genetic algorithm combined with density functional theory is used to perform an extensive global search of the potential energy surface to locate the global minima (GM) and low-lying isomers. For each ligand, the structural features are roughly similar to $(AuSR)_n$, that is, the GMs change from single ring to catenane structures. Besides, a new folding mode (ring-at-ring) is revealed in the GMs at n = 12–13. The GM structures are very similar for L = SH and SCH_3 and for L = PH_2 and $P(CH_3)_2$, which indicate that the R groups can be directly replaced by H in the calculations. However, there are obvious differences in the GM structures for L = Cl, SH and PH_2. It is found that the origin of the ligand effects is the polarity of the Au–L bond. The Au–Cl bond is of the highest plorarity, and the noncovalent interaction index approach reveals that the Au···Au aurophilic interaction is the strongest for L = Cl, followed by L = SH and L = PH_2. Moreover, the polarity of the Au–L bond may affect the preferred Au–L–Au bond angle, which is an important geometric parameter. The linearity of Cl–Au–Cl is the easiest to be broken for more Au···Au contacts, which is viewed in the GMs of $(AuCl)_n$ at n = 7, 8 and 12.

Received 29th October 2015
Accepted 22nd December 2015

DOI: 10.1039/c5ra22741k

www.rsc.org/advances

I. Introduction

Ligand-protected gold nanoparticles (Au_mL_n) have attracted considerable interest because of their promising applications in nanocatalysis, medicine and optical devices.[1–7] Among the Au_mL_n clusters, thiolate protected gold nanoclusters, $Au_m(SR)_n$, are the most studied systems. Two breakthroughs for $Au_m(SR)_n$ clusters are the crystal structure determinations of $Au_{102}(SR)_{44}$ and $Au_{25}(SR)_{18}$ clusters, which consist of $Au_n(SR)_{n+1}$ (n = 1, 2) oligomers that bind to a gold core with high symmetry.[8,9] Subsequently, based on this model of a gold core surrounded by gold thiolate oligomers, density functional theory (DFT) calculations were used to predict the structures of $Au_{38}(SR)_{24}$,[10–14] $Au_{24}(SR)_{20}$,[15,16] and $Au_{144}(SR)_{60}$.[17–21] Recent studies found that the structures of $Au_{68}(SR)_{30}$ cluster and $Au_{18}(SC_6H_{11})_{14}$ are still consistent with this model of a gold core surrounded by gold thiolate oligomers.[22–24] Moreover, several experimental studies have revealed the ligand effects on the stabilities and properties of noble metal clusters. The redox properties of $Au_{38}(SPhX)_{24}$ clusters and the original magic stability of $Au_m(SR)_n$ clusters was demonstrated by employing ligand effects.[25,26] Recently, Johnson *et al.*[27] studied the effect of phosphine substitution on ligand reactivity and binding, and it is shown that several larger clusters readily undergo exchange of the PPh_3 ligands in solution for singly substituted PPh_2Me and PPh_2Cy ligands. With the experimental observations on the ligand effects on Au nanoclusters, many theoretical calculations have been performed to understand how surface ligands influence the electronic structure and stability of metal nanoclusters. Ligand effects on the structure and electronic optical properties of $Au_{25}(SR)_{18}^-$ clusters have been explored and the studies have revealed that *p*-thiophenolates ligands that include electron-withdrawing groups could result in the distortion of the $Au_{25}S_{18}$ framework.[28] $Au_{38}(SR)_{24}$, $Au_{102}(SR)_{44}$ and $Au_{24}(SR)_{20}$ have been also employed to study the ligand effects on stability, and it was found that –SPhCOOH has more favorable binding than –SPh and –SPhF.[29–32] Recently, the role of the anchor atom and ligand types on the properties of $Au_m(SR)_n$ nanoclusters have been studied, and there was a more pronounced effect on the gold–ligand unit structure and ultimately on the aurophilic interactions.[33,34]

Department of Chemistry, Anhui University, Hefei, Anhui, 230601, China. E-mail: clj@ustc.edu

† Electronic supplementary information (ESI) available: The atomic coordinates (in Å) of the global minimum and low-energy structures of $(AuL)_n$ (L = Cl, SH, SCH_3, PH_2, $P(CH_3)_2$, n = 1–13) clusters. See DOI: 10.1039/c5ra22741k

The aforementioned ligand effects are mainly on $Au_{102}(SR)_{44}$ and $Au_{25}(SR)_{18}$ clusters with a gold-to-ligand ratio greater than 1 : 1. Previous studies also made some progress in the homoleptic type of –SR and $–PR_2$ group protected Au clusters. The cyclic oligomers of $[Au(PR_2)]_n$ (n = 3, 4 and 6) have been synthesized and characterized.[35–37] The lowest-energy isomers of $(AuCl)_n$ (n = 3–6) clusters are also found to be cyclic arrangements.[38] The synthetic $Au_{10}(SR)_{10}$ and $Au_{12}(SR)_{12}$ clusters were found to be composed of two interpenetrating pentagons and hexagons, respectively.[39] Gronbeck and co-workers explored the low-lying structures of $(AuSR)_n$ with n = 2–12 and predicted a transition from planar rings to crown structures.[40] The structures of $(AuSR)_n$ (n = 6–12) clusters were relocated using the DFT and MP2 methods and a new structural family of double helical conformations was discovered.[41]

Despite the significant progresses in the area of Au_mL_n clusters, size evolution and ligand effects on $(AuL)_n$ clusters with an Au-to-L ratio of 1 : 1 still lack systematic investigations because of the limited experimental data on these structures. To the best of our knowledge, literature on the ligand effects of $(AuL)_n$ clusters is rare. Herein, we seek to investigate the ligand effects on the size evolution of $(AuL)_n$ clusters, with n = 1–13, L = Cl, SH, SCH_3, PH_2 and $P(CH_3)_2$. The DFT method combined with genetic algorithm (GA) is used to locate the global minimum (GM) structures of the clusters. To explore the origin of the ligand effects, the polarity of bonds, aurophilicity and binding energies of the clusters are also discussed.

II. Computational details

The global minimum search for the $(AuL)_n$ clusters was carried out using GA coupled with DFT, which has been successfully applied in the structural prediction of a number of systems.[42–45] GA is an optimization strategy that is inspired by the Darwinian evolution, which mimics the process of natural selection.[46–48] This strategy is routinely used to generate useful solutions for optimization and search problems. GA belongs to the larger class of evolutionary algorithms, which generate solutions to optimization problems using the techniques inspired by natural evolution such as inheritance, mutation, selection, and crossover. Starting with a population of candidate structures, we relax these candidates to the nearest local minimum. Using the relaxed energies as the criteria, a fraction of the population is selected as "parents". The next generation of candidate structures is the structure matching the "parents". This progress is repeated until the GMs are located.[49] The TPSSh functional[50] is selected for DFT calculation, which has been proven to be reliable in the prediction of ligand-protected Au nanoclusters.[51,52] The unbiased global search of the potential energy surface at the DFT level is very time-consuming. Thus, in the global search procedure, we chose small basis sets, 3-21G for Cl, S, P, C, and H and Lanl2MB for Au, in the DFT calculations to save time. With a small basis set, all the possible motifs can be found, but the energy sequences of various isomers are different. Then, the obtained low-lying geometries are fully relaxed at the TPSSh/6-311G*/LANL2TZ(f) level after global optimization. The normal mode frequencies are also computed at the same level for all the structures to ensure that they belong to the minima, and all the minima are verified by the absence of an imaginary frequency. All the DFT calculations were carried out using the GAUSSIAN 09 package.[53]

III. Results and discussion

In this study, the GMs and low-lying isomers of $(AuL)_n$ (L = Cl, SH, SCH_3, PH_2 and $P(CH_3)_2$, n = 1–13) are located at the TPSSh/6-311G*/LANL2TZ(f) level, which include single-ring, helical, crown, catenane and double-ring structures. Then, to investigate size evolution and ligand effects, the average binding energies, aurophilicity and the polarity of the bonds are discussed.

1. Geometric structures

We first introduce the geometric structures of $(AuSCH_3)_n$ (n = 1–13) clusters (Fig. 1a), which have been reported before for n = 2–12.[26,27] All the known GMs are reproduced in our study. **2a** is a fold line, which is 0.47 eV lower in energy than the previous rhombic isomer. When n = 3–9, the single rings are the GMs. However, **3a** is a planar single ring, while **4a** and **5a** are twisted single rings. The GMs are all helical structures at n = 6–9. In particular, **8a** and **8b** are competitive isomers, and **8a** lies only 0.02 eV lower in energy than **8b** (a double-ring structure consisting of two four-membered rings). When n = 10-12, the GMs are all catenane structures consisting of two interpenetrating five-/six-membered rings. It is worth noting that **12b** and **12a** are nearly degenerated in energy. Interestingly, **12b** has a unique ring-at-ring structure (a small Au_4L_4 ring inserted into a large Au_8L_8 ring), which has not been reported before. **13a** is also a catenane structure, which is composed of five- and eight-membered interpenetrating rings. The crown isomers with high symmetries are also shown in Fig. 1a, which lie much high in energy at large sizes.

In most calculations, the large –SR groups in experiments are often replaced by an $–SCH_3$ group to reduce the computation cost.[54] Thus, can the $–SCH_3$ group be further replaced by the –SH group in calculations? Fig. 1b plots the GMs and low-energy isomers of $(AuSH)_n$ clusters. It can be seen that the values for $(AuSH)_n$ clusters are in agreement with those of $(AuSCH_3)_n$ clusters in the GM structures, except for n = 8, where the energy sequence changes slightly. The double-ring and helical structure are also competitive in energy at n = 8, where the former (**8A**) is 0.01 eV lower in energy for L = SH but is 0.02 eV higher in energy for L = SCH_3. Due to the great similarity between the structures of $(AuSH)_n$ and $(AuSCH_3)_n$, it can be expected that the –SR groups can be simplified directly to the –SH group in calculations for the structural prediction of $Au_m(SR)_n$ complexes.

To explore the ligand effects, we locate the GMs of $(AuL)_n$ clusters with the $–SCH_3$ group replaced by the $–P(CH_3)_2$ group. Fig. 2a displays the GMs and low-energy structures of the $[AuP(CH_3)_2]_n$ clusters. From this figure, we can see that the frameworks of the $(AuSCH_3)_n$ and $[AuP(CH_3)_2]_n$ clusters are very similar. However, the planar single rings are global minimum up to n = 5, and the GMs prefer crown structures at n = 6–8 in

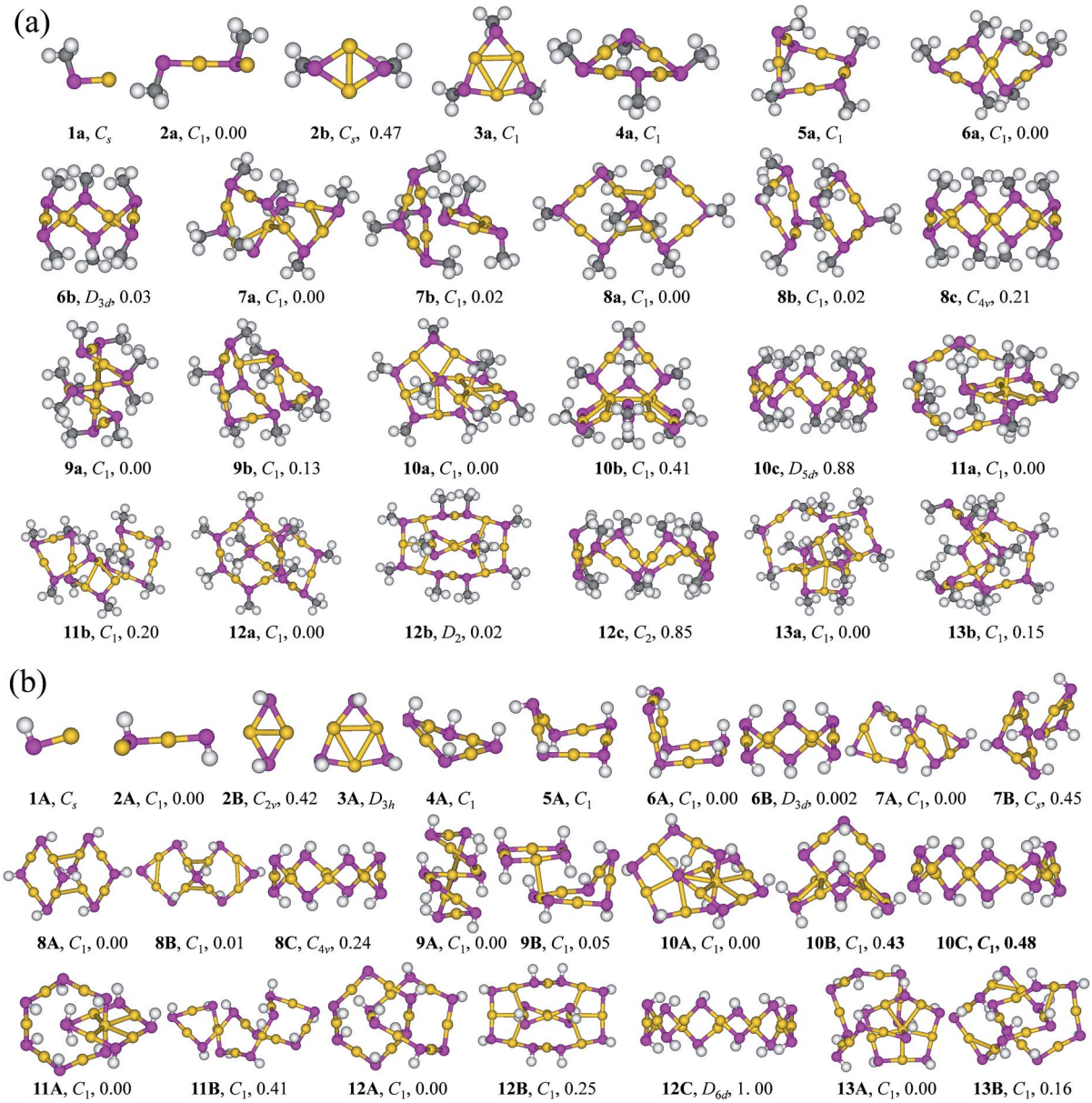

Fig. 1 Optimized geometries of (a) $(AuSCH_3)_n$ and (b) $(AuSH)_n$ ($n = 1$–13) clusters at the TPSSh/6-311G* (S, H, C) and Lanl2TZ(f) (Au) levels. Au-yellow, S-purple, H-white, and C-gray.

$[AuP(CH_3)_2]_n$. Moreover, the GM of $[AuP(CH_3)_2]_{12}$ (**12I**) is a catenane structure consisting of five- and seven-membered rings instead of two six-membered rings in $(AuSCH_3)_{12}$.

In Fig. 2b, we can see that the GMs of $(AuPH_2)_n$ are very similar to those of $[AuP(CH_3)_2]_n$ clusters. The difference is that the GM of $(AuPH_2)_9$ is a crown structure, whereas the GM of $(AuPH_2)_{13}$ is a ring-at-ring structure (a small Au_5L_5 ring inserted into a large Au_8L_8 ring). Due to the great similarity between $(AuPH_2)_n$ and $[AuP(CH_3)_2]_n$, the large $-PR_2$ groups in experiments can be simplified by the $-PH_2$ group in calculations.

Due to practical reasons, there is no report on the synthesis of Cl-protected gold nanoclusters. However, sometimes the –SR and $-PR_2$ ligands can be replaced by the –Cl group for theoretical computations to predict structures in calculations.[55,56] The GMs and low-lying structures of $(AuCl)_n$ clusters are given in Fig. 3. It can be seen that $(AuCl)_n$ clusters also have certain similarities with $(AuSCH_3)_n$ clusters in the structures. When n ranges from 3 to 5, the GMs present single rings, while when $n = 6$ and 9 helical structures are formed. When $n = 10$ and 11, the GMs are catenane structures. Obviously, the GMs have unique structures at $n = 7$, 8, 12, and 13 and the energy sequences also change compared with $(AuSCH_3)_n$ clusters. Concretely, $\mathbf{7X_1}$ is a double-ring structure consisting of three- and four-membered rings, and one edge of the three-membered ring is broken. Similarly, the three-membered rings in $\mathbf{8X_1}$ are broken to bring the Au atoms close to each other. $\mathbf{12X_1}$ is a ring-at-ring structure (an Au_4Cl_4 ring inserted into an Au_8Cl_8 ring); however, the linearity of two Cl–Au–Cl edges in the Au_8Cl_8 unit is broken to 110°. $\mathbf{13X_1}$ is an irregular structure

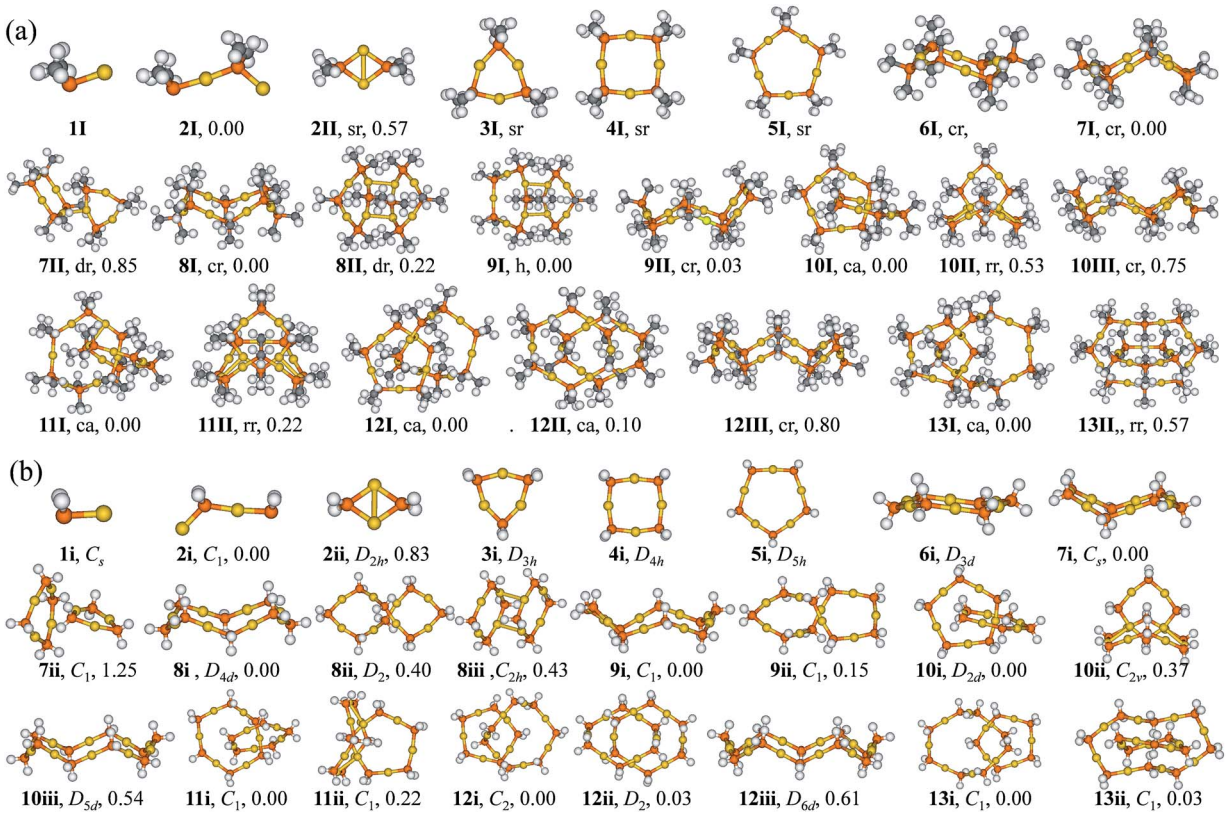

Fig. 2 Optimized geometries of (a) $[AuP(CH_3)_2]_n$ and (b) $(AuPH_2)_n$ (n = 1–13) clusters at the TPSSh/6-311G* (P, C, H) and Lanl2tz(f) (Au) levels. Au-yellow, P-orange, H-white, and C-gray. The labels are sr: single ring, cr: crown, dr: double ring, h: helix, and ca: catenane.

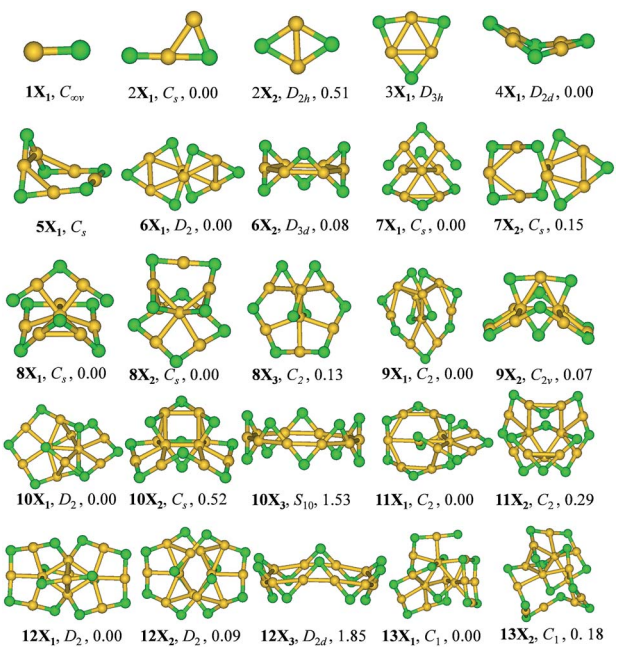

Fig. 3 Optimized geometries of $(AuCl)_n$ (n = 1–13) at the TPSSh/6-311G* (Cl) and Lanl2tz(f) (Au) levels. Au-yellow and Cl-green.

with a broken four-membered interpenetrating ring. The reason for the serious breaking of the Cl–Au–Cl linearity at n = 7, 8, 12 and 13 is to have more Au···Au contacts.

2. Binding energies

Based on the structural analysis mentioned above, it is found that $(AuL)_n$ clusters with different ligand types show certain differences in their structures. To explore ligand effects on the stability, the average binding energies (E_b) per AuL unit of each GM cluster were calculated, which is defined as $E_b = (nE_{Au} + nE_L - E_{(AuL)n})/n$, where E_{Au}, E_L and $E_{(AuL)n}$ are the energies of Au, L and $(AuL)_n$, respectively. Fig. 4a compares E_b as a function of cluster size for the five ligands. It is clearly seen that there is an increment in E_b for the successive addition of one AuL unit. For L = Cl, SH and SCH_3, E_b increases quickly up to n = 3, and then converges at n = 4. For L = PH_2 and $P(CH_3)_2$, E_b increases quickly with n up to 4, and then converges at n = 5. For each ligand, E_b reaches the highest value at n = 10 (Fig. 4b), thus indicating magic stability of the structure with two interpenetrating five-membered rings. From the curves of E_b, the order of stability for each ligand should be SH > Cl > PH_2 > SCH_3 > $P(CH_3)_2$. $(AuSH)_n$ is obviously more stable than $(AuSCH_3)_n$ at a large size, which may be due to the weak hydrogen bond (S···H–S) in the former. For L = PH_2, SCH_3 and $P(CH_3)_2$, the small stability differences may be due to the steric effects of the $-CH_3$ group.

To show the size evolution more clearly for L = Cl, SH, and PH_2, the relative energies of the total binding energies (E) and their fitting (E_{fit}) are plotted in Fig. 4c–e in a manner that emphasizes particular stable minima or "magic numbers". In

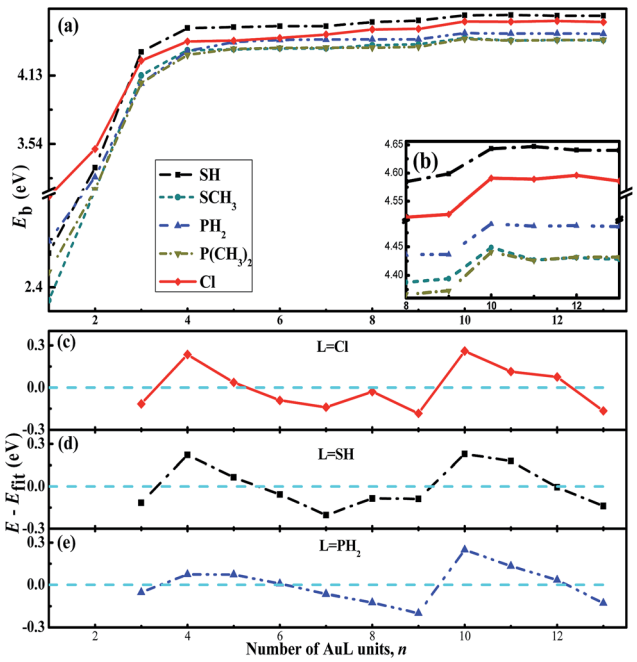

Fig. 4 (a) Binding energy of the GMs of $(AuL)_n$ (L = Cl, SH, SCH_3, PH_2, $P(CH_3)_2$) clusters as the function of cluster size, n. (b) Enlarged binding energy of the GMs of $(AuL)_n$ (L = Cl, SH, SCH_3, PH_2, and $P(CH_3)_2$) clusters in the 8–13 region. (c–e) Plots of the energetic gaps ($E - E_{fit}$) of the lowest-energy $(AuL)_n$ (L = Cl, SH, PH_2) clusters as a function of cluster size, where E is the total energy and E_{fit} is a four-parameter fit of the GMs: $E_{fit} = a - bn^{1/3} + cn^{2/3} + dn$ (related coefficient $R > 0.999$).

these curves, positive peaks correspond to more stable structures. It can be seen that, for each ligand, there are two pronounced peaks at $n = 4$ and 10, which indicate that $(AuL)_4$ and $(AuL)_{10}$ are more stable than their neighbors. For L = Cl, there is a small peak at $n = 8$, which indicates the stability of the double-ring $(AuCl)_8$ cluster. It should be noted that the stability of $(AuPH_2)_5$ is similar to that of $(AuPH_2)_4$, which manifests the stability of five-membered ring. This results in the highest relative stability of $(AuPH_2)_{10}$ among the three ligands.

3. Aurophilicity

Previous studies suggested that the strong Au···Au aurophilic interaction is responsible for the stability of closed-chain gold thiolate $[Au(SC_6H_4\text{-}p\text{-}CMe_3)]_{10}$,[37,38] and these catenane structures can give rise to the largest number of close Au···Au contacts, resulting in lower energies. For large cluster sizes ($n \geq 10$) of these systems, it is found that most of the GMs are catenane structures. For L = Cl, the linearity of the Cl–Au–Cl bonds is broken at $n = 7$, 8 and 12 to have more Au···Au contacts due to aurophilicity. However, aurophilicity is a type of weak noncovalent interaction, and cannot be studied directly by the natural bonding orbital methods. Herein, we use the noncovalent interaction (NCI) index approach to detect aurophilicity based on electron density and its derivatives,[57,58] which has been successfully applied to investigate the aurophilic interaction in $(Au_2S)_n$ clusters.[59] The NCI studies were carried out using Multiwfn package,[60] and the NCI isosurface images were created using VMD.[61] The NCI index is based on the reduced density gradient, s, and the electron density, ρ, where

$$s = \frac{1}{2(3\pi^2)^{1/3}} \frac{|\nabla\rho|}{\rho^{4/3}}$$

and it allows to highlight interactions characterized by a low-density regime. To distinguish different types of interactions, the second Hessian eigenvalue (λ_2) can be used as a sign, which can be either positive or negative.

Fig. 5 plots the reduced density gradient (s) *versus* electron density (ρ) multiplied by the sign of λ_2 and the low-gradient ($s = 0.30$ au) NCI isosurfaces of the three typical structures $(AuCl)_{10}$ (**10X$_1$**), $(AuSH)_{10}$ (**10A**) and $(AuPH_2)_{10}$ (**10i**). From the left part of Fig. 5, the low density, low-gradient spikes lie at about sign $(\lambda_2)\rho = -0.035$ au for $(AuCl)_{10}$, -0.032 au for $(AuSH)_{10}$ and -0.020 au for $(AuPH_2)_{10}$, which represent strong noncovalent attractions, and the more negative spikes represent stronger attractions (Au···Au aurophilic interactions between the central gold atoms in each ring and those on the periphery). The Au···Au aurophilic interactions can be viewed directly from the NCI isosurfaces in the right part of Fig. 5, where the darkness of the color indicates the strength of the Au···Au aurophilicity (Cl > SH > PH_2). Besides, the average Au···Au distances in the $(AuCl)_{10}$, $(AuSH)_{10}$ and $(AuPH_2)_{10}$ clusters are 2.96 Å, 3.04 Å, and 3.34 Å, respectively, which agree well with the relative strength of the Au···Au aurophilic interactions within them. Moreover, for the $(AuCl)_{10}$ and $(AuSH)_{10}$ clusters, there are smaller spikes at about sign $(\lambda_2)\rho = -0.025$ au and -0.020 au, respectively, which represent another Au···Au aurophilic interaction (between gold atoms around the periphery, as viewed in the NCI isosurfaces). The average Au···Au distances between the gold atoms around the periphery are 3.11 Å and 3.30 Å for L = Cl and SH, respectively, which are in agreement with their relative strength. In

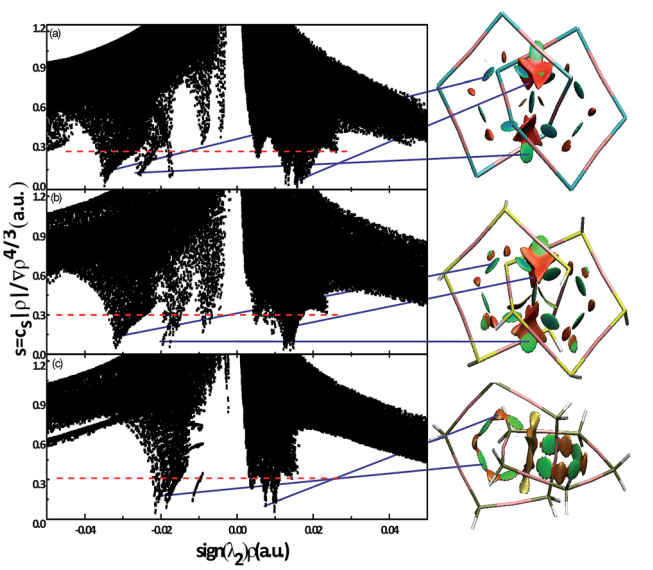

Fig. 5 Plots of reduced density gradient *versus* electron density multiplied by the sign of the second Hessian eigenvalue (left) and NCI isosurfaces at $s = 0.30$ (right) for the global minimum structures of (a) $(AuCl)_{10}$, (b) $(AuSH)_{10}$ and (c) $(AuPH_2)_{10}$.

particular, both $(AuSH)_{10}$ and $(AuPH_2)_{10}$ have low density spikes at sign $(\lambda_2)\rho = -0.020$ au, and the average Au···Au distances are close to each other. This further shows that the Au···Au distance is in agreement with the relative strength of the Au···Au aurophilic interactions. In addition, the spikes at positive values represent steric interactions between the two rings, which are the red regions of the isosurfaces. In comparison, Fig. 5a and b based on $(AuCl)_{10}$ and $(AuSH)_{10}$, respectively, are almost the same. This trend is also somewhat reflected in the calculated geometrical parameters reported in Table 1, and also in the average Au···Au distances of 2.96 and 3.04 Å. However, the $(AuPH_2)_{10}$ cluster shows differences in all these properties.

4. Polarity and bond angles

Previous comparisons show that the aurophilicity in the $(AuCl)_n$ cluster is the strongest, followed by $(AuSH)_n$ and $(AuPH_2)_n$. As is well known, the order for the polarity of the Au–L bonds is Au–Cl > Au–SH > Au–PH_2. Thus, the aurophilicity may be affected by the polarity of Au–L bonds. To verify the Au–L bond polarity in the different homoleptic gold clusters, a natural bonding orbital (NBO) analysis[62–64] was performed on the single-ring structures. The results are shown in Fig. 6, where the polarity of an Au–L bond is represented as the percentage of the shared electron pairs due to L. For $(AuL)_n$ ($n = 1$), Au and L atoms supply one electron each to form one Au–L bond, and the polarity of the Au–Cl, Au–S and Au–P bonds are 0.75, 0.66, 0.56, respectively, indicating that the charge is polarized towards L. When $n \geq 2$, each L contributes three electrons and each Au contributes one electron to form $2n$ Au–L bonds, thus the polarity increases suddenly at $n = 2$, and then levels off at $n > 2$. Due to the larger electronegativity difference between Au and Cl atoms, the polarity of the Au–Cl bonds is stronger than Au–S and Au–P bonds, which is in accordance with the relative strength of Au···Au aurophilic interactions. Moreover, stronger polarity can result in weaker covalency, which can make it easier for the linearity of L–Au–L bonds to be broken. For L = Cl, because of the strongest polarity and aurophilicity, the linearity of Cl–Au–Cl bonds is the easiest to be broken for more Au···Au aurophilic contacts, which is found in the GMs of $(AuCl)_7$, $(AuCl)_8$, $(AuCl)_{12}$ and $(AuCl)_{13}$.

Moreover, due to the difference in polarity for Au–L bonds, the preferred angles of Au–L–Au bonds are different, which further affects their structures. Table 1 compares the changes in Au–L–Au angles for the monocyclic structures of these three systems. For small cluster sizes, the Au–Cl–Au, Au–S–Au and Au–P–Au angles show substantial contractions from the ideal 79°, 89° and 120°, respectively. The Au–Cl–Au angles reach the ideal values at $n = 3$–4 for L = Cl, $n = 4$ for L = SH, and $n = 5$–6 for L = PH_2. Thus, $(AuCl)_4$, $(AuSH)_4$ and $(AuPH_2)_5$ with ideal Au–L–Au angles are more stable than their neighbors.

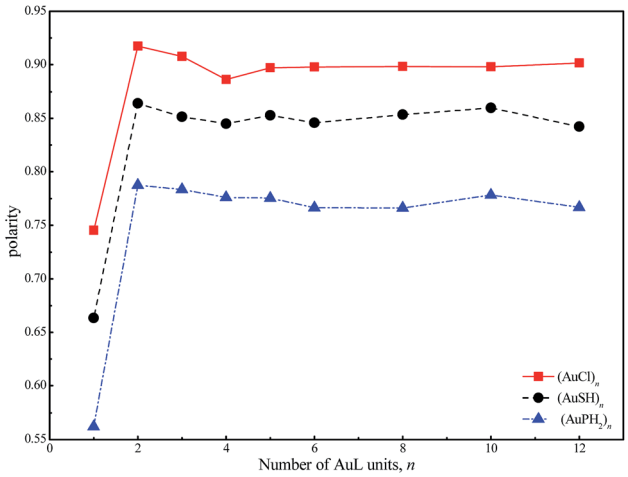

Fig. 6 Polarity of Au–L bond in monocyclic $(AuL)_n$ clusters (L = Cl, SH, and PH_2) as the function of cluster size, n.

IV. Conclusions

In the present study, the size evolution and ligand effects of $(AuL)_n$ clusters with n = 1–13, L = Cl, SH, SCH_3, PH_2, and $P(CH_3)_2$, are investigated using a method that combined the GA with DFT. The GMs of $(AuSCH_3)_n$ shift from single rings at n = 2–9 to catenane structures at $n \geq 10$, which is in agreement with the previous studies. Besides, a new folding mode (ring-at-ring) is revealed in the GMs at n = 12–13. When the ligands are SH, PH_2 and $P(CH_3)_2$, the structural features are roughly similar to those of $(AuSCH_3)_n$. Thus, the –SCH_3 group can be replaced by the –SH group, which suggests a way to predict the structures of $Au_m(SR)_n$ by exploring $Au_m(SH)_n$ clusters. Similarly, the large –PR_2 groups in experiments can be directly simplified by –PH_2

Table 1 Comparison of bond angles for the monocyclic structures of $(AuCl)_n$, $(AuSH)_n$ and $(AuPH_2)_n$ clusters

	$(AuCl)_n$			$(AuSH)_n$			$(AuPH_2)_n$	
N	Au–Cl–Au (°)	Cl–Au–Cl (°)	N	Au–S–Au (°)	S–Au–S (°)	N	Au–P–Au (°)	P–Au–P (°)
$2X_2$	64.2	115.8	**2B**	65.4	114.6	**2ii**	73.4	106.6
$3X_1$	74.5	165.5	**3A**	77.2	162.8	**3i**	88.4	151.6
$4X_1$	87.4	177.4	**4A**	87.5	178.2	**4i**	104	166.0
$5X_1$	78.7–95.8	177.7	**5A**	94.6	177.3	**5i**	114.1	173.9
$6X_2$	79.8	178.5	**6A**	87.6	178.8	**6i**	119	177.7
$8X_3$	79.2	178.9	**8C**	88.1	178.2	**8i**	119.7	179.0
$10X_3$	79.2	179.1	**10C**	88.9	177.9	**10iii**	120	179.5
$12X_3$	79.2	179.3	**12C**	89.5	177.8	**12iii**	120.1	179.8

group in calculations. For L = Cl, most of the GMs are also single rings and catenane structures, but the linearity of Cl–Au–Cl is broken at $n = 7$, 8, 12 and 13 to have more Au···Au contacts due to the aurophilicity.

The NCI method reveals that the aurophilicity in the $(AuCl)_n$ cluster is the strongest, followed by $(AuSH)_n$ and $(AuPH_2)_n$, which is accompanied by the lengthening of the Au···Au distances. The polarity of Au–L bonds is the strongest for L = Cl among these three ligands, which is in accordance with the relative strength of Au···Au aurophilic interactions and further results in breaking of the Cl–Au–Cl linearity in some GM structures. The polarity could also affect the preference of Au–L–Au angles and further results in the difference of structures. $(AuCl)_4$, $(AuSH)_4$ and $(AuPH_2)_5$ with ideal Au–L–Au angles are more stable than their neighbors. This results in the highest relative stability of $(AuPH_2)_{10}$ among the three ligands.

Ligand effects are frequently viewed in the experimentally produced ligand-protected Au clusters. Taking $(AuL)_n$ clusters as examples, this study tried to answer the question of how ligands affect these structures. The origin is the polarity of the Au–L bond, which results in gaps in the strength of Au···Au aurophilic interactions and in the preferred Au–L–Au angles.

Acknowledgements

This study is supported by the National Natural Science Foundation of China (Grant No. 21273008, 21573001). The calculations are carried out in the High-Performance Computing Center of Anhui University.

References

1 B. K. Juluri, Y. B. Zheng, D. Ahmed, L. Jensen and T. J. Huang, *J. Phys. Chem. C*, 2008, **112**, 7309–7317.
2 Y. B. Zheng, L. Jensen, W. Yan, T. R. Walker, B. K. Juluri, L. Jensen and T. J. Huang, *J. Phys. Chem. C*, 2009, **113**, 7019–7024.
3 A. Tcherniak, S. Dominguez Medina, W. S. Chang, P. Swanglap, L. S. Slaughter, C. F. Landes and S. Link, *J. Phys. Chem. C*, 2011, **115**, 15938–15949.
4 M. Draper, I. M. Saez, S. J. Cowling, P. Gai, B. Heinrich, B. Donnio, D. Guillon and J. W. Goodby, *Adv. Funct. Mater.*, 2011, **21**, 1260–1278.
5 T. V. Basova, R. G. Parkhomenko, I. K. Igumenov, A. Hassan, M. Durmus, A. G. Gurek and V. Ahsen, *Dyes Pigm.*, 2014, **111**, 58–63.
6 H. C. Weissker, R. L. Whetten and X. Lopez-Lozano, *Phys. Chem. Chem. Phys.*, 2014, **16**, 12495–12502.
7 Q. Hao, B. K. Juluri, Y. B. Zheng, B. Wang, I. K. Chiang, L. Jensen, V. Crespi, P. C. Eklund and T. J. Huang, *J. Phys. Chem. C*, 2010, **114**, 18059–18066.
8 P. D. Jadzinsky, G. Calero, C. J. Ackerson, D. A. Bushnell and R. D. Kornberg, *Science*, 2007, **318**, 430–433.
9 J. Akola, M. Walter, R. L. Whetten, H. Hakkinen and H. Grönbeck, *J. Am. Chem. Soc.*, 2008, **130**, 3756–3757.
10 H. Hakkinen, R. Barnett and U. Landman, *Phys. Rev. Lett.*, 1999, **82**, 3264.
11 H. Qian, Y. Zhu and R. Jin, *ACS Nano*, 2009, **3**, 3795–3803.
12 Y. Pei, Y. Gao and X. C. Zeng, *J. Am. Chem. Soc.*, 2008, **130**, 7830–7832.
13 S. Knoppe, A. C. Dharmaratne, E. Schreiner, A. Dass and T. Bürgi, *J. Am. Chem. Soc.*, 2010, **132**, 16783–16789.
14 O. Lopez-Acevedo, H. Tsunoyama, T. Tsukuda and C. M. Aikens, *J. Am. Chem. Soc.*, 2010, **132**, 8210–8218.
15 Y. Pei, R. Pal, C. Liu, Y. Gao, Z. Zhang and X. C. Zeng, *J. Am. Chem. Soc.*, 2012, **134**, 3015–3024.
16 M. Zhu, H. Qian and R. Jin, *J. Phys. Chem. Lett.*, 2010, **1**, 1003–1007.
17 H. Qian and R. Jin, *Chem. Mater.*, 2011, **23**, 2209–2217.
18 S. Malola and H. Hakkinen, *J. Phys. Chem. Lett.*, 2011, **2**, 2316–2321.
19 H. Qian and R. Jin, *Nano Lett.*, 2009, **9**, 4083–4087.
20 J. Z. Sexton and C. J. Ackerson, *J. Phys. Chem. C*, 2010, **114**, 16037–16042.
21 C. Yi, M. A. Tofanelli, C. J. Ackerson and K. L. Knappenberger Jr, *J. Am. Chem. Soc.*, 2013, **135**, 18222–18228.
22 M. Azubel, J. Koivisto, S. Malola, D. Bushnell, G. L. Hura, A. L. Koh, H. Tsunoyama, T. Tsukuda, M. Pettersson and H. Hakkinen, *Science*, 2014, **345**, 909–912.
23 A. Das, C. Liu, H. Y. Byun, K. Nobusada, S. Zhao, N. Rosi and R. Jin, *Angew. Chem.*, 2015, **127**, 3183–3187.
24 S. Chen, S. Wang, J. Zhong, Y. Song, J. Zhang, H. Sheng, Y. Pei and M. Zhu, *Angew. Chem., Int. Ed.*, 2015, **54**, 3145–3149.
25 R. Guo and R. W. Murray, *J. Am. Chem. Soc.*, 2005, **127**, 12140–12143.
26 Y. Negishi, N. K. Chaki, Y. Shichibu, R. L. Whetten and T. Tsukuda, *J. Am. Chem. Soc.*, 2007, **129**, 11322–11323.
27 G. E. Johnson, A. Olivares, D. Hill and J. Laskin, *Phys. Chem. Chem. Phys.*, 2015, **17**, 14636–14646.
28 A. Tlahuice-Flores, R. L. Whetten and M. Jose-Yacaman, *J. Phys. Chem. C*, 2013, **117**, 20867–20875.
29 J. Jung, S. Kang and Y. K. Han, *Nanoscale*, 2012, **4**, 4206–4210.
30 Y. Gao, *J. Phys. Chem. C*, 2013, **117**, 8983–8988.
31 Q. Tang, R. Ouyang, Z. Tian and D. E. Jiang, *Nanoscale*, 2015, **7**, 2225–2229.
32 T. W. Ni, M. A. Tofanelli, B. D. Phillips and C. J. Ackerson, *Inorg. Chem.*, 2014, **53**, 6500–6502.
33 E. Pohjolainen, H. Hakkinen and A. Clayborne, *J. Phys. Chem. C*, 2015, **119**, 9587–9594.
34 J. Zhong, X. Tang, J. Tang, J. Su and Y. Pei, *J. Phys. Chem. C*, 2015, **119**, 9205–9214.
35 D. M. Stefanescu, H. F. Yuen, D. S. Glueck, J. A. Golen and A. L. Rheingold, *Angew. Chem., Int. Ed.*, 2003, **42**, 1046–1048.
36 D. M. Stefanescu, H. F. Yuen, D. S. Glueck, J. A. Golen, L. N. Zakharov, C. D. Incarvito and A. L. Rheingold, *Inorg. Chem.*, 2003, **42**, 8891–8901.
37 D. M. Stefanescu, D. S. Glueck, R. Siegel and R. E. Wasylishen, *Langmuir*, 2004, **20**, 10379–10381.
38 F. Rabilloud, *J. Comput. Chem.*, 2012, **33**, 2083–2091.
39 M. R. Wiseman, P. A. Marsh, P. T. Bishop, B. J. Brisdon and M. F. Mahon, *J. Am. Chem. Soc.*, 2000, **122**, 12598–12599.
40 H. Gronbeck, M. Walter and H. Hakkinen, *J. Am. Chem. Soc.*, 2006, **128**, 10268–10275.

41 N. Shao, Y. Pei, Y. Gao and X. C. Zeng, *J. Phys. Chem. A*, 2009, **113**, 629–632.
42 Y. Yuan and L. Cheng, *J. Chem. Phys.*, 2012, **137**, 044308.
43 Y. Yuan and L. Cheng, *Int. J. Quantum Chem.*, 2012, **113**, 1264–1271.
44 Y. Yuan, L. Cheng and J. Yang, *J. Phys. Chem. C*, 2013, **117**, 13276–13282.
45 L. Li and L. Cheng, *J. Chem. Phys.*, 2013, **138**, 094312.
46 R. L. Johnston, *Dalton Trans.*, 2003, 4193–4207.
47 A. Shayeghi, D. Götz, J. Davis, R. Schaefer and R. L. Johnston, *Phys. Chem. Chem. Phys.*, 2015, **17**, 2104–2112.
48 D. M. Deaven and K. M. Ho, *Phys. Rev. Lett.*, 1995, **75**, 288–291.
49 S. Hamad, C. Catlow, S. Woodley, S. Lago and J. Mejias, *J. Phys. Chem. B*, 2005, **109**, 15741–15748.
50 M. Mantina, R. Valero and D. G. Truhlar, *J. Chem. Phys.*, 2009, **131**, 64706.
51 Y. K. Shi, Z. H. Li and K. N. Fan, *J. Phys. Chem. A*, 2010, **114**, 10297–10308.
52 L. Cheng, Y. Yuan, X. Zhang and J. Yang, *Angew. Chem., Int. Ed.*, 2013, **52**, 9035–9039.
53 M. Frisch, G. Trucks, H. B. Schlegel, G. Scuseria, M. Robb, J. Cheeseman, G. Scalmani, V. Barone, B. Mennucci and G. Petersson, *Gaussian 09, Revision B. 01*, Gaussian Inc., Wallingford, CT, 2010.
54 J. A. Howell, *Polyhedron*, 2006, **25**, 2993–3005.
55 D. E. Jiang and M. Walter, *Nanoscale*, 2012, **4**, 4234.
56 Z. M. Tian and L. J. Cheng, *Phys. Chem. Chem. Phys.*, 2015, **17**, 13421.
57 E. R. Johnson, S. Keinan, P. Mori-Sanchez, J. Contreras-Garcia, A. J. Cohen and W. Yang, *J. Am. Chem. Soc.*, 2010, **132**, 6498–6506.
58 J. Contreras-García, E. R. Johnson, S. Keinan, R. Chaudret, J. P. Piquemal, D. N. Beratan and W. Yang, *J. Chem. Theory Comput.*, 2011, **7**, 625–632.
59 Y. Q. Feng and L. J. Cheng, *RSC Adv.*, 2015, **5**, 62543.
60 T. Lu and F. Chen, *J. Comput. Chem.*, 2012, **33**, 580–592.
61 W. Humphrey, A. Dalke and K. Schulten, *J. Mol. Graphics*, 1996, **14**, 33–38.
62 J. Foster and F. Weinhold, *J. Am. Chem. Soc.*, 1980, **102**, 7211–7218.
63 F. Weinhold and C. R. Landis, *Valency and bonding: a natural bond orbital donor-acceptor perspective*, Cambridge University Press, Cambridge, 2005.
64 A. E. Reed, L. A. Curtiss and F. Weinhold, *Chem. Rev.*, 1988, **88**, 899–926.